Available online at www.sciencedirect.com
ScienceDirect
Journal of Power Sources 175 (2008) 482–489
JOURNAL OF POWER SOURCES
www.elsevier.com/locate/jpowsour

Production of hydrogen by ethanol steam reforming on Co/Al_2O_3 catalysts: Effect of addition of small quantities of noble metals

Luciene P.R. Profeti, Edson A. Ticianelli, Elisabete M. Assaf*

Universidade de São Paulo, Instituto de Química de São Carlos, CEP 13560-970, São Carlos, SP, Brazil

Received 8 August 2007; received in revised form 14 September 2007; accepted 17 September 2007
Available online 22 September 2007

Abstract

The catalytic performance of Co/Al_2O_3 catalysts promoted with small amounts noble metals (Pt, Pd, Ru, Ir) for steam reforming of ethanol (SRE) has been investigated. The catalysts were characterized by the energy dispersive X-ray, X-ray diffraction, BET surface area, X-ray absorption fine structure and temperature reduction programmed techniques. The results showed that the promoting effect of noble metals included a marked decrease of the reduction temperatures of both Co_3O_4 and cobalt surface species interacting with the support due to the hydrogen spillover effect, leading to a significant increase of the reducibilities of the promoted catalysts. The better catalytic performance for the ethanol steam reforming at 400 °C was obtained for the $CoRu/Al_2O_3$ catalyst, which presented an effluent gaseous mixture with the highest H_2 selectivity and the reasonable low CO formation.

Keywords: Cobalt; Promoters; Hydrogen; Ethanol; Steam reforming

1. Introduction

The use of hydrogen for fuel cells applications is one of the most interesting non-polluting methods for the production of electrical energy, either for automotive or stationary scale usages. However, the use of hydrogen fuel cells in vehicles or in portable power plants needs light weight H_2 storage systems or the on-board reforming of organic compounds containing hydrogen. There are several source fuels for hydrogen production from reforming, including gasoline [1], methane [2], methanol [3], etc., but ethanol is more attractive because of its natural availability, non-toxicity, safe storage and handling. Additionally, ethanol can be produced from several biomass sources; in particular in Brazil ethanol is already produced and distributed through the gas station network for thermal engine cars.

Thermodynamic studies have shown that the steam reforming of ethanol is feasible at temperatures higher than 230 °C with the main products being CO_2 and H_2 [4]. Despite of the stoichiometry reaction for maximum hydrogen production is very simple:

$$C_2H_5OH + 3H_2O \rightarrow 6H_2 + 2CO_2, \quad \Delta H_{298\,K} = +347.4\,kJ\,mol^{-1} \tag{1}$$

The steam reforming of ethanol involves a complex reaction pathway and the selectivity for hydrogen is affected by many undesirable side reactions. The presence of some reaction intermediates decreases the hydrogen production efficiency and can reduce the operation time of the catalyst. For instance, the side reactions involve dehydration or dehydrogenation of the ethanol molecule producing intermediate products such as ethylene, which is easily transformed into a carbon deposit onto the catalyst [5]. Also, the reaction mechanism is dependent on the catalyst used [6].

In previous studies, several catalysts have been proposed for ethanol steam reforming for hydrogen production, such as Rh [7], Pt [8], Pd [9], Ni [10], Co [11,12], immobilized on different supports (Al_2O_3, SiO_2, TiO_2, La_2O_3, etc.). Among them, Co seems very appropriate because of its high activity and low cost [13,14]. Some studies performed by Haga et al. [15] have shown that the Co/Al_2O_3 catalyst is active and selective for the steam reforming of ethanol at 400 °C, yielding 8 and 6% CO and CH_4, respectively. In addition, Batista et al. [16–18] investigated Co

* Corresponding author. Tel.: +55 16 33739951; fax: +55 16 33739952.
E-mail address: eassaf@iqsc.usp.br (E.M. Assaf).

0378-7753/$ – see front matter © 2007 Published by Elsevier B.V.
doi:10.1016/j.jpowsour.2007.09.050

catalysts at different loadings dispersed on different material supports for the steam reforming of ethanol at 400 °C. The results obtained showed a conversion near to 100% for ethanol and an average gaseous composition of 67% H_2, 24% CO_2, 9% CH_4 and 800 ppm of CO. Furthermore, they observed that the Co 18%/Al_2O_3 shows the best catalytic performance with higher CO removal.

Recently, it has been demonstrated that the activity of Co catalyst can be increased with the addition of low contents of noble metals, for applications on the catalytic removal of CO and NO from fuels [19,20] and Fischer–Tropsch synthesis [21–23]. However, the evaluation of the performance of such catalysts for the ethanol steam reforming towards hydrogen production is not yet considered. In this context, the present work investigates Co/Al_2O_3 catalysts promoted with platinum, palladium, iridium and ruthenium at low contents with respect to their physical properties and the activity in the catalysis of ethanol steam reforming.

2. Experimental

2.1. Catalyst preparation

The catalysts were prepared by successive wet impregnations, as follows. The γ-Al_2O_3 pellets were previously sieved to 80–65 mesh particle size and treated at 550 °C for 3 h under synthetic air flow, in order to remove adsorbed contaminants. A given amount of $Co(NO_3)_2{\cdot}6H_2O$ (98%, Aldrich) aqueous solution was first impregnated on the γ-Al_2O_3 powder by solvent evaporation in a rotating evaporator. The mixture was dried at 100 °C, and then calcined in air at 550 °C for 6 h. The load of Co in the catalysts was 18% (w/w).

The promoter metals were added on the Co/Al_2O_3 calcined samples from aqueous solutions containing Pt ($H_2PtCl_6{\cdot}2H_2O$, Aldrich), or Pd ($PdCl_2$, Aldrich), or Ru ($RuCl_3{\cdot}H_2O$, Aldrich), or Ir ($IrCl_4{\cdot}H_2O$, Aldrich). The solvent was evaporated and the precipitated calcined in air at 550 °C for 5 h, i.e., the same impregnation method previously used. All the promoted catalysts contained 0.3 wt.% of noble metal.

2.2. Sample characterization

2.2.1. Energy dispersive X-ray (EDX) and X-ray diffraction (XRD)

The catalyst chemical compositions were determined by EDX analyses, using a Leo 440 microscope linked to an Oxford 7060 microanalyzer, with the samples immobilized on an Al support. The crystalline structures of the catalysts were investigated by XRD performed on a Rigaku Multiflex diffractometer using a Cu Kα (1.5406 Å) radiation source. The X-ray diffractograms were obtained for 2θ values ranging from 20° to 70°.

The mean sizes of the oxide particles were determined from the X-ray diffractograms, using the Scherrer equation and assuming that the particles are spherical:

$$L = \frac{0.9\lambda}{B_{2\theta}\cos\theta_{\max}} \quad (2)$$

where λ is the X-ray wavelength (1.54056 Å for the Cu Kα radiation), $B_{2\theta}$ the width of the diffraction peak at half-height and $\theta_{\max}$ is the angle at the peak maximum position.

The Co_3O_4 particle sizes were converted to the respective cobalt particle sizes after their reduction according to Eq. (3) [21,24], which takes an $d(Co^0)$ the relative molar volume of metallic cobalt and Co_3O_4:

$$d(Co^0) = 0.75d(Co_3O_4) \quad (3)$$

The dispersion of cobalt in the catalyst was estimated the from cobalt metal particle sizes, assuming that the particles are spherical and uniform with a site density of 14.6 atoms nm^{-2} [25], as follows:

$$D\,(\%) = \frac{96}{d\,(\mathrm{nm})} \quad (4)$$

2.2.2. Surface area and porosity measurements

The surface area, the pore diameter and the pore volume were determined by N_2 physisorption at 77 K using a Quantachrome Nova 2.0 equipment. The surface area was calculated by the Brunauer–Emmett–Teller (BET) isotherm and the pore diameter was determined by the Barret–Joyner–Halenda (BJH) method. All catalyst samples were outgased for 2 h before the measurements.

2.2.3. Temperature programmed reduction (TPR)

The TPR measurements were performed in a reactor with a quartz U-shaped tube with a mixture of H_2 (1.96%)/Ar at 30 mL min^{-1}. The catalyst sample (50 mg) was heated from room temperature to 1000 °C at a rate of 10 °C min^{-1}. The water produced during the reduction was removed by driving the effluent gas through a tube containing silica gel. The outlet gas was analyzed by a thermal conductivity detector (TCD) and the H_2 consumption was measured quantitatively. The amount of consumed hydrogen was determined by comparing its peak area to the area of a standard CuO sample.

2.2.4. X-ray absorption near edge structure (XANES)

The catalysts were studied by the XANES technique at Co K-edge (7709 eV). The spectra were recorded on the XAFS beam line in the National Synchrotron Light Source Laboratory (LNLS), Brazil. The samples were pressed into pellets for this experiment. The data acquisition system comprised three ionization detectors (incidence I_0, transmitted I_t and reference I_r). Nitrogen was used in the I_0, I_t and I_r chambers, and a Si(1 1 1) synglecrystal of third-order was used as monochromator. The reference channel was employed primarily for internal calibration of the edge position by using a pure Co foil. The XANES spectra were analyzed using the WinXAS software.

2.3. Catalytic tests

The catalytic tests for ethanol steam reforming were performed in a fixed-bed system with a continuous reactant flow (13 mm diameter). The reaction temperature was measured by

Table 1
Characterization of the catalysts

Catalyst	Co[a] (wt.%)	Co[b] particle size (nm)	dCo^0 (nm)	D (%)	BET surface area ($m^2\ g^{-1}$)	Pore diameter (nm)	Pore volume ($cm^3\ g^{-1}$)	H_2[c] (mmol g^{-1})
Co/Al_2O_3	18	12.8	9.6	10	125.1	4.0	0.11	2.16
$CoPt/Al_2O_3$	20	15.1	11.3	8.5	123.0	4.6	0.12	2.75
$CoPd/Al_2O_3$	22	14.3	10.8	9.0	113.7	4.2	0.11	2.95
$CoIr/Al_2O_3$	19	15.1	11.4	8.5	111.2	4.4	0.12	2.40
$CoRu/Al_2O_3$	18	14.3	10.8	8.9	114.8	2.8	0.11	2.52

[a] Determined by EDX.
[b] Determined by XRD.
[c] Determined by TPR.

a thermocouple placed closed to the catalyst. The catalytic tests were performed continuously for 6 h.

The catalyst (150 mg) was previously reduced in situ with pure H_2 (30 mL min^{-1}) at 600 °C for 1 h. After this step, the reactor was cleaned with N_2 and the water–ethanol mixture (molar ratio 3:1) was fed at a rate of 2.5 $cm^3\ h^{-1}$ after it was pumped into a heated chamber (180 °C) and vaporized. The gaseous product composition of the reactor effluent was analyzed on line by gas chromatography using a Varian, model 3800 equipment with two thermal conductivity detectors, a 13× molecular sieve packed (H_2 analyses) and a Porapack-N columns (CO_2, CO and CH_4 analysis). The liquid products were condensed in the reactor outlet and analyzed by gas chromatography (Hewlett Packard 5890) with a flame ionic detector (FID) and a capillary column HP-FFAP.

The catalytic activity was evaluated in terms of the distribution of the gaseous products (S) defined as follows:

$$S\,(\%) = \left(\frac{M_P}{M_{\Sigma P}}\right) \times 100 \quad (4)$$

where M_P is the number of moles of each product and $M_{\Sigma P}$ is the sum of the number of moles of all gaseous products.

3. Results and discussion

3.1. EDX analysis

The catalysts compositions were quantitatively analyzed by EDX at three different points on the catalyst sample providing the average cobalt and noble metals contents. Table 1 shows the average atomic percentage of the catalysts, where it is seen that the values are very close to the nominal composition of Co in all regions, suggesting that preparation method leaded the required homogeneous distribution of this metal. The amount added of the promoter metal was very small (0.3%, w/w), and so it was only possible to verify qualitatively the presence of the noble metal. The values in Table 1 were consistent with the nominal compositions. Furthermore, the EDX analyses of the fresh samples evidenced that no detectable Cl was present in the catalysts.

3.2. DRX analysis

The crystalline phases formed after the catalyst preparation processes of were identified by XRD. Fig. 1 shows the X-ray diffractograms of the promoted catalysts compared to that for Co/Al_2O_3. The presence of the low intensity diffraction peaks at $2\theta = 46.2°$ and 66.9° observed for all supported Co catalysts, is attributed to γ-Al_2O_3 with low crystallinity [14]. The peaks located at $2\theta = 31.3°$, 36.8°, 44.9°, 59°.3 and 65.3° can be attributed either to the Co_3O_4 ($CoO_x{\cdot}Co_2O_3$) or the $CoAl_2O_4$ species [14,16–18]. The cobalt aluminate might be possibly formed by the diffusion of Co^{2+} ions into the Al_2O_3 support, where they may occupy tetrahedral or octahedral lattice sites [21]. Because both $CoAl_2O_4$ and Co_3O_4 have a cubic spinel structure with almost the same XRD patterns, the presence of the $CoAl_2O_4$ phase is not fully demonstrated. However, the appearance of the peak at $2\theta = 44.9°$, observed for all samples, is a good evidence of the presence of Co_3O_4.

Comparing the diffractograms of the promoted with that of the unpromoted catalysts it is possible to note that there are no significant differences in the crystalline structure of materials. This feature is due to the incorporation of the noble metals predominantly on the Co/Al_2O_3 particle surfaces, with a large

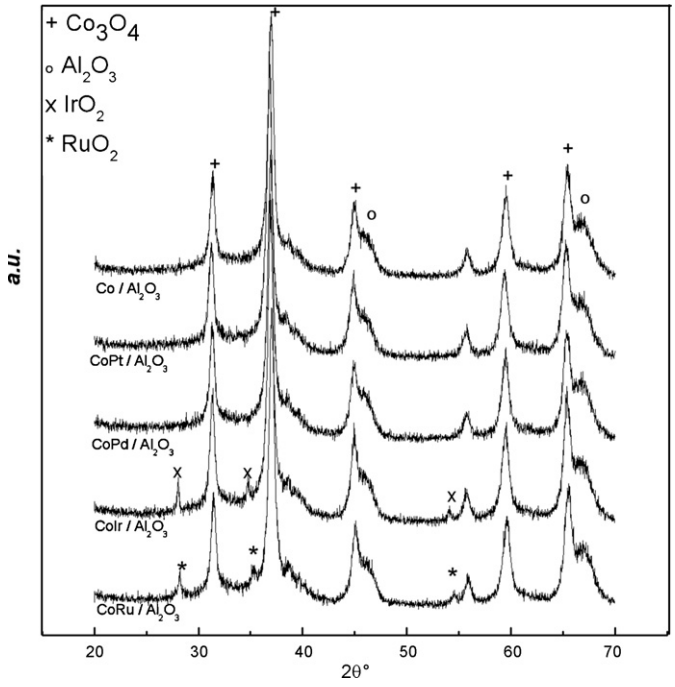

Fig. 1. X-ray diffractograms of the unpromoted and promoted Co/Al_2O_3 catalysts.

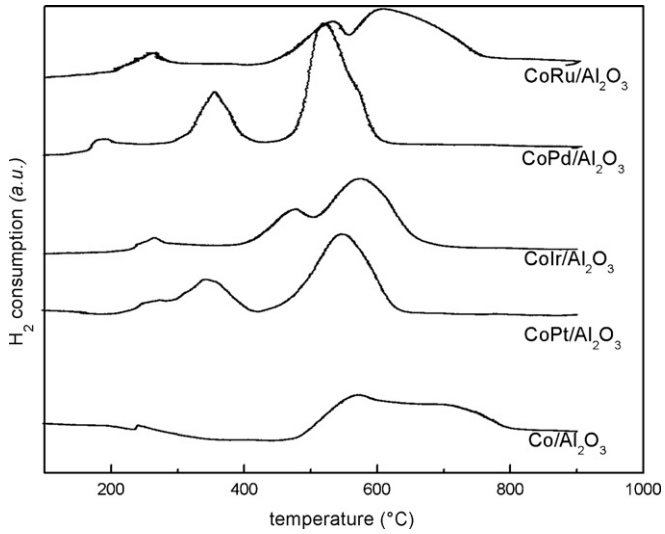

Fig. 2. TPR profiles of the promoted and unpromoted Co/Al_2O_3 catalysts.

dispersion. The diffractograms of the catalysts promoted with Ir and Ru showed additional peaks with lower intensities, which indicate the formation of RuO_2 and IrO_2 with tetragonal structure. Tetragonal RuO_2 presents diffraction peaks at $2\theta = 28°$, 35°, 40.5°, 54.3° and 59.5° (RuO_2, JCPDS card no. 40-1290), while those for IrO_2 are at $2\theta = 28°$, 34.7°, 40.2°, 54° and 58.5° (IrO_2, JCPDS card no. 43-1019). No peaks attributed to Pt and Pd species were observed probably due to their larger degree of dispersion in the catalysts.

The average Co_3O_4 crystallite sizes, estimated using the Scherrer's formula, are shown in Table 1. For the Co/Al_2O_3 catalyst, the average Co_3O_4 crystallite size is 12.8 nm, which corresponds to 9.6 nm when reduced to the Co metal. After the addition of the noble metals, the average Co_3O_4 crystallite size increased a little. Such phenomenon must be caused by the second calcination process, necessary for the incorporation of the metal promoter. The cobalt dispersion estimated from the diffractograms resulted between 8 and 10% (Table 1).

3.3. BET surface area

Results of specific surface area, pore volume and average pore diameter measurements are shown in Table 1. There were no significant changes on the values of the pore volume and the average pore diameter with the noble metal addition. However, the surface area undergoes a small decrease for Co/Al_2O_3 catalyst with Pd, Ru and Ir contents, suggesting that the second calcinations process for the noble metal addition contributes to the surface area decrease, as also evidenced by XRD from the increase of the crystallite size.

3.4. Temperature programmed reduction

TPR profiles were obtained aiming to investigate the oxide phases present on the catalysts, as well as to evaluate the thermal stability of these phases. Fig. 2 shows the reduction profiles of the promoted and unpromoted catalysts, where several hydrogen consumption bands resulting from the superposition of reduction peaks can be observed. All curves shown in Fig. 2 have a small peak bellow 300 °C, which is an evidence of the incomplete thermal decomposition of the nitrate ions coming from the cobalt precursor [26]. The nitrate ion interacts strongly with the alumina support, which difficult its complete thermal decomposition.

The TPR curve for the Co/Al_2O_3 catalyst shows that the reduction begins at ca. 500 °C, and reaches a maximum of hydrogen consumption nearly 570 °C followed by a broad peak with the center at ca. 700 °C. This reduction profile agrees with those in the literatures [14,16,17,27], where the presence of two reduction peaks, one at ~350 °C and another located between 400 and 700 °C is reported. Some differences in these temperatures are expected taking into account the differences in the experimental conditions of data acquisition, such as the flow rate of the gaseous mixture, the heating rates, etc., besides some influence of the sample reproducibility [27].

Even though there are several TPR studies of Co/Al_2O_3 catalysts, there are still important disagreements about the attribution of the reduction peaks. Some authors suggest that the peak at the lower temperatures corresponds to the reduction of large crystalline Co_3O_4 particles to Co^0 via CoO formation [28,24]. Other researches propose that these low temperatures peak is ascribed to the reduction of Co_3O_4 to CoO, with only a small portion of the CoO reducing to Co^0 [22,23]. In any case, the Co_3O_4 species include those weakly bonded on the support, since for pure Co_3O_4 there is only one sharp reduction peak at 378 °C [20]. Despite these controversies, there is an agreement in the peaks attribution at higher temperatures. In this case, the process corresponds to the reduction of Co^{3+} and Co^{2+} species, which are highly dispersed on the surface and strongly interacting with Al_2O_3. The Co^{3+} and Co^{2+} species form aluminate compounds due to the occurrence of solid-state reactions during the calcination process [20,22,23,28].

Supposing that the first step corresponds to the reduction of Co_3O_4 to CoO (Eq. (5)) and the second step to the reduction of CoO to Co^0 (Eq. (6)), the theoretical ratio of peak area of the first to the second peaks in the TPR profiles should be 1:3 [27]. This ratio is obtained for the Co/Al_2O_3 reduction profile shown in Fig. 2, indicating that the Co_3O_4 to Co^0 reduction follows the reactions:

$$Co_3O_4 + H_2 \rightarrow 3CoO + H_2O \quad (5)$$

$$3CoO + 3H_2 \rightarrow 3Co + 3H_2O \quad (6)$$

The addition of the noble metals leads to significant changes in the TPR profiles of the Co/Al_2O_3 catalyst. In the $CoPt/Al_2O_3$ reduction profile there are two well-defined peaks located at temperatures lower than those observed for Co/Al_2O_3. This behavior indicates that the Pt facilitates the reduction of either the Co_3O_4 or the cobalt surface species interacting with the support. Another point to consider is that the reduction peak located at ~330 °C is close to the reduction peak of Pt/Al_2O_3 [8]. So, this first reduction peak may be assigned to the reduction of Pt oxide/Co_3O_4 species weakly bonded on support [20]. The second peak at ca. 550 °C must correspond to the reduction of

Co_3O_4 with lower interaction with Pt. The sample with Pd presented a profile similar to that with Pt, however, the peaks are more intense, indicating higher hydrogen consumption during this reduction process.

The samples promoted with Ru and Ir showed lower reduction temperatures compared to those for the unpromoted catalyst. Also, there is smaller separation between the first and the second reduction peak compared to the results for the samples with Pt and Pd. This feature may be caused by a high interaction of cobalt with ruthenium or iridium, leading to the formation of mixed oxides [29]. Thus, it is suggested that the first reduction peak, observed at both TPR profiles ($CoRu/Al_2O_3$ and $CoIr/Al_2O_3$), corresponds to the reduction of Ru or Ir oxides with high interactions with Co_3O_4 and the second reduction peak, located at higher temperatures, is attributed to the reduction of cobalt species with lower interaction with RuO_2 or IrO_2 particles.

The behaviors of the TPR curves of the promoted catalysts may result from a hydrogen spillover phenomenon that occurs in the noble metals [21–23]. On the promoted catalysts, the hydrogen is firstly dissociated on the reduced noble metal clusters and converted to active hydrogen, which can migrate, reducing the neighboring cobalt oxide clusters. These results indicate that the presence of noble metal makes easier the reduction of cobalt species.

In order to estimate quantitatively the effect of noble metal addition on the Co/Al_2O_3 catalyst, the amount of H_2 consumption during the reduction process was calculated from the TPR responses (listed in Table 1) and the sequence of this effect is CoPd > CoPt > CoRu > CoIr > Co. These results demonstrate that the amount of reducible cobalt species in Co/Al_2O_3 is smaller than those in the promoted catalysts. This enhancement of reducibility can be closely related to the improvements in catalytic performances for the promoted catalysts, as seen below.

3.5. XANES analyses

X-ray absorption experiments were performed on freshly calcined catalysts samples in the XANES region at Co K-edge (7709 eV). The XANES method is often applied in order to identify the oxidation state and obtain qualitative information about the local geometry around a selected element in a sample. In this study, the XANES spectra were used to obtain information about the influence of the noble metal addition on oxidation state of the cobalt species present in the catalysts.

Fig. 3 shows normalized XANES spectra for the catalysts, compared to those of standard Co metal, CoO and Co_3O_4. K-edge spectra for 3D transition metals or compounds may involve the X-ray-induced energy dependent successive promotion of a 1s electron into valence shells, higher energy bound states and into the continuum. In centrosymmetric bond environments, the lowest energy transition involving 1s–3d excitations is symmetry-forbidden. However, in lower symmetry structures, valence shell d–p mixing allows enhanced intensity for these transitions. At energies above the 1s–3d excitations, the principal rising edge occurs, which can include transitions to higher energy bound states such as 1s–4p and 1s–*n*p. Multiple scattering features and another resonance transition features may also occur in this energy region, particularly for metal oxides. In the present work in all cases the pre-edge feature appears at ca. 7710 eV, while the main absorption edge is observed at ca. 7725–7730 eV.

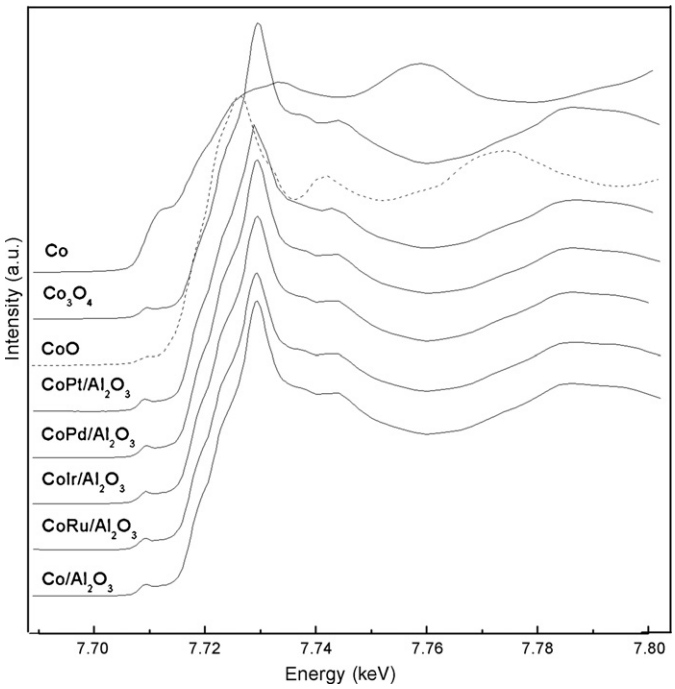

Fig. 3. Normalized XANES spectra of Co K-edge of the samples and reference compounds.

The XANES spectra for all catalysts showed the pre-edge characteristics and main absorption peak very similar to those of the Co_3O_4 XANES spectrum. The energy of the main edge (7729 eV) is close to the value reported by Jacobs et al. [23,30] and Vrastald et al. [31] for Co_3O_4 and Co/Al_2O_3 catalysts, and remarkably different from the value reported for the $CoAl_2O_4$ edge energy [32]. Moreover, the XANES spectrum for the $CoAl_2O_4$ compound shows a stronger pre-edge peak as compared to those in the Co_3O_4 species [31]. So, the conclusion is that no characteristics assigned to cobalt species from aluminate were found in the XANES spectra obtained for the promoted and unpromoted cobalt catalysts. This analysis is in agreement with the XRD data, where Co_3O_4 was found as the major species present on the catalysts.

In order to quantify the presence of the different phases on the Co/Al_2O_3 catalysts, the linear combination (LC) of the XANES spectra was performed comparing the profiles of the reference compounds (Co_3O_4 and CoO) with those of the catalysts, as shown in Fig. 4. It was found that the CoO and Co_3O_4 contribute with 6.07 and 93.92%, respectively to the Co/Al_3O_4 XANES spectrum (Fig. 4). For the promoted catalysts, the fittings are very similar to that of the unpromoted catalyst indicating that no changes occur in the oxidation states of Co due to the noble metals addition.

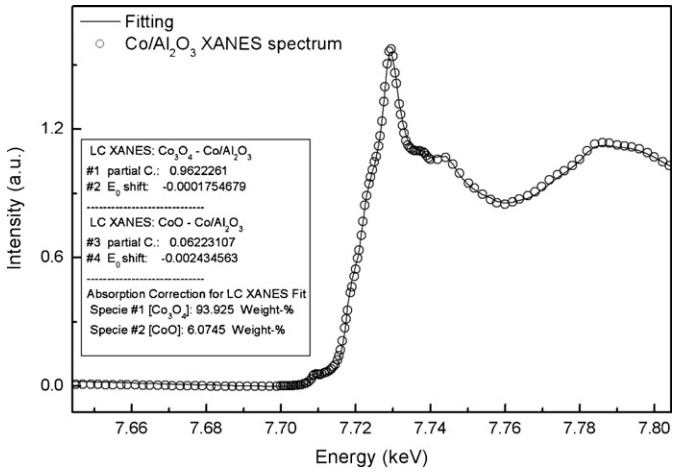

Fig. 4. LC XANES fitting of the Co/Al_2O_3 catalysts spectrum and the reference compounds (CoO and Co_3O_4).

3.6. Catalytic tests

In order to investigate the catalytic activity of the materials for the ethanol steam reforming, tests were performed at two different temperatures (400 and 500 °C), in both cases using a 3:1 water/ethanol molar ratio. The support γ-Al_2O_3 and the catalysts containing the noble metals 0.3 wt.% dispersed in γ-Al_2O_3 showed only ethene formation.

As expected, the conversion of ethanol increases with the increase of temperature becoming close to 100% at 500 °C, whereas at 400 °C the ethanol conversion values were around of 70%. The addition of the noble metal slightly enhanced the catalytic activity; hence an effect pronounced was observed on the gaseous distribution.

In all measurements, gaseous mixtures containing H_2 at higher proportion and smaller amounts of CH_4, CO, CO_2 and C_2H_4 were obtained. Figs. 5 and 6 present the distribution of these gaseous products as a function of time, for the reaction occurring at 400 °C. It is important to emphasize that, for feeding a fuel cell, it is necessary a gaseous mixture rich in H_2 with low CO concentration and the unconverted ethanol may be returned to the reactor.

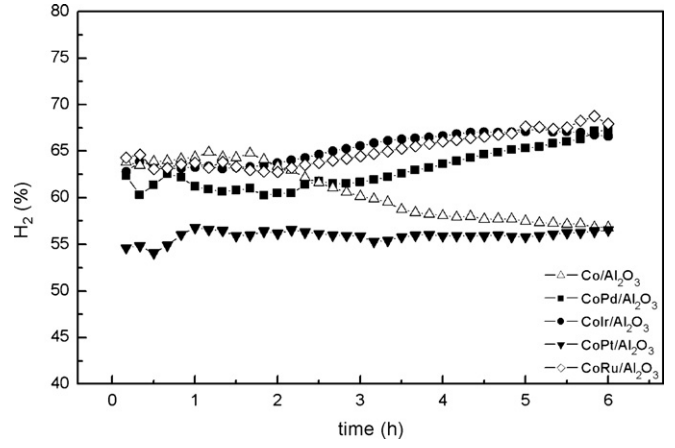

Fig. 5. Hydrogen formation for the unpromoted and promoted Co/Al_2O_3 catalysts at 400 °C.

It is clearly seen that, the reaction products changes with the catalyst composition. In Fig. 5 it is observed that at the beginning, the H_2 production for the Co/Al_2O_3 catalyst is about 63%, but this decreases progressively until 57% after 6 h. For the Pd, Ru and Ir promoted catalysts the H_2 production was 65% at the beginning of the experiments, but this is followed by a progressive increase at the end of experiments. The lowest H_2 production was obtained for the catalyst with Pt, which yielded 55% H_2 remaining approximately constant until the end of experiment.

Fig. 6A and B shows the CO and CO_2 productions for all the catalysts at 400 °C. The catalysts promoted Pd, Pt and Ir have shown CO production higher than the unpromoted one, whereas $CoRu/Al_2O_3$ presented the smallest CO formation when compared to the other cases. Additionally, a higher CO_2 production was obtained by the promoted catalysts, particularly for $CoRu/Al_2O_3$, as observed in Fig. 6B. Moreover, the CO production for all the catalysts decreases with time on stream, whereas the CO_2 formation slightly increases, excepting for the Co/Al_2O_3. This behavior is an indication that the metallic sites may be acting for both the ethanol reform and for the water gas shift (WGS) reaction (reaction (7)) at this temperature.

$$CO + H_2O \rightleftharpoons H_2 + CO_2 \quad (7)$$

Besides H_2, CO and CO_2, the formation of CH_4 and C_2H_4 was noted with amounts depending on the catalyst composition (Fig. 6C and D). It has been proposed that the formation of methane occurs either via methanation of CO (reaction (8)) or via partial ethanol decomposition (reaction (9)) [5]:

$$CO + 3H_2 \rightarrow CH_4 + H_2O \quad (8)$$

$$C_2H_5OH \rightarrow CH_4 + CO + H_2 \quad (9)$$

The methanation reaction is thermodynamically favored at temperatures below 530 °C, while the rate of ethanol decomposition always increases with the increase of temperature [5]. The presence of CH_4 in the reaction products is undesirable because it diminishes the hydrogen yield, since that the H_2 would be consumed for the process [5].

The ethene production was also dependent on the catalyst composition. C_2H_4 formation occurs due to the dehydration of ethanol (reaction (10)) taking place in the acidic sites of the alumina support [5]:

$$C_2H_5OH \rightarrow C_2H_4 + H_2O \quad (10)$$

Moreover, ethene is a precursor of the formation of carbon species, since it undergoes polymerization reactions to form coke, which causes the deactivation of catalysts, as well as the decrease of the selectivity toward H_2 production.

Fig. 6D shows that production of ethene for Co/Al_2O_3 is higher than that for the others promoted catalysts. A high selectivity toward ethene is indicative of a poorer coverage of the alumina surface, leading more exposition of acidic sites. However, it appears that not only the exposure of acidic sites, but

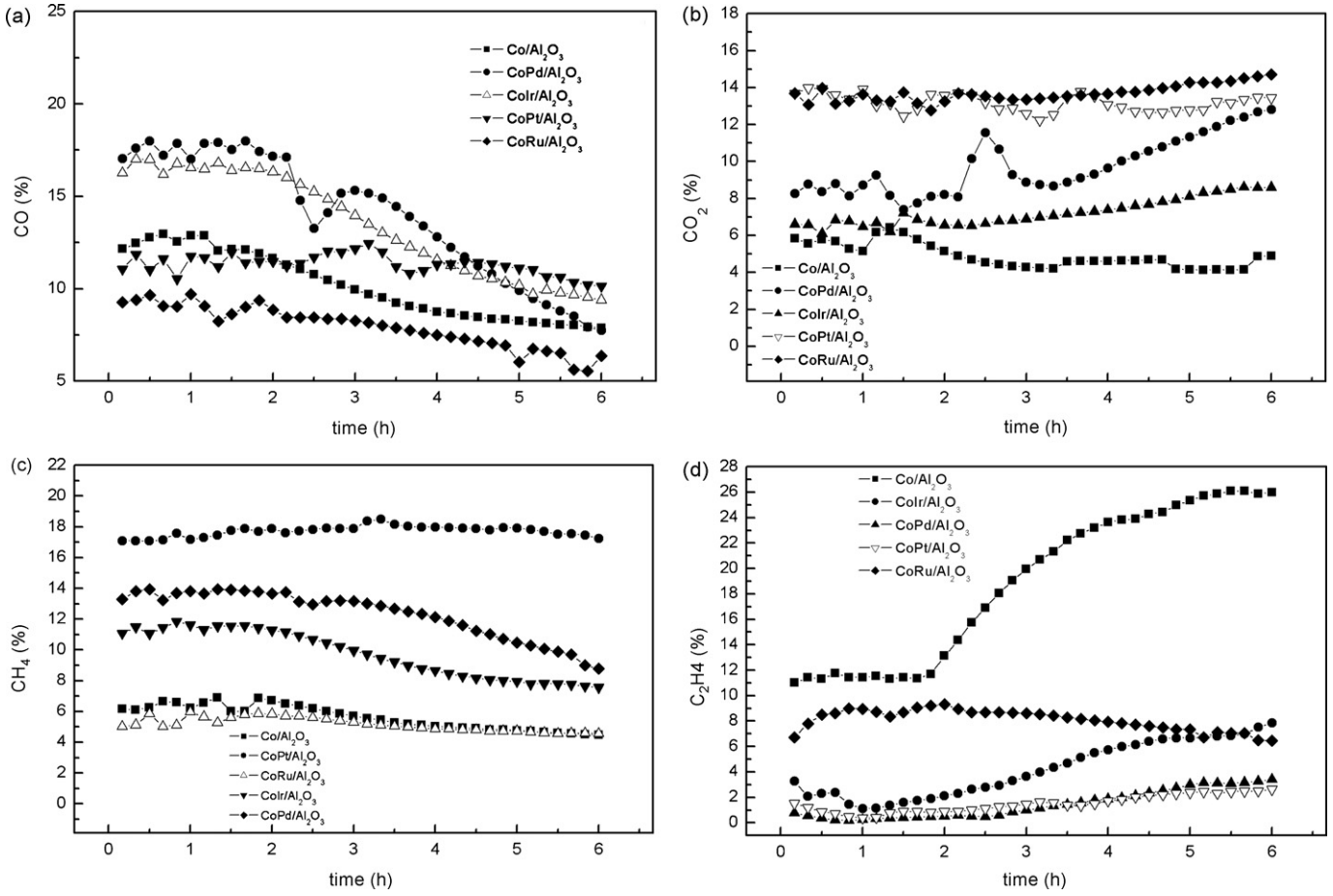

Fig. 6. Formation of gaseous by-products and reaction intermediates for the promoted and unpromoted Co/Al_2O_3 catalysts at 400 °C: (A) CO, (B) CO_2, (C) CH_4 and (D) C_2H_4 production.

also the nature of the metallic species and their interaction with cobalt species are important requirement to diminish the undesirable formation of ethene. Probably, this is the reason why the catalyst samples promoted with Pt and Pd leaded to a smaller formation of ethene (Fig. 6D).

Furthermore, it is noteworthy the decrease in H_2 production for Co/Al_2O_3 catalyst concomitantly with the increase of the ethene production along the reaction. This behavior suggests that catalyst deactivation occur with time on stream, probably due to coking or reoxidation of the Co sites. Indeed, the formation of solid products, such as carbonaceous species (coke), was observed for all the reforming reactions ranging between 2.5 and 3.5 mmol h^{-1}. However, in the case of the promoted catalysts, even though the coke formation, the decrease of hydrogen production it was not observed. Thereby, the addition of the noble metals on the Co/Al_2O_3 catalyst probably led to a more stable metallic state and less susceptible to the deactivation process by reoxidation during the reforming reaction.

Table 2 summarizes the distribution of these products at the end of the experiment (6 h) for 400 and 500 °C. The H_2, CO and CH_4 productions decreased with the increase of temperature, whereas the CO_2 and C_2H_4 formation was superior at this temperature. The formation of small amounts of liquid products (less than 1%) such as acetaldehyde, ethyl ether, acetone, acetic acid and ethyl acetate, at both temperatures was also observed.

Table 2
Distribution of gaseous products after 6 h of ethanol steam reforming of unpromoted and promoted Co/Al_2O_3 catalysts

Catalyst	H_2 (%)		CO (%)		CO_2 (%)		CH_4 (%)		C_2H_4 (%)	
	400 °C	500 °C	400 °C	500 °C	400 °C	500 °C	400 °C	500 °C	400 °C	500 °C
Co/Al_2O_3	56	55	8	3	5	20	4	3	26	16
$CoPt/Al_2O_3$	56	59	10	4	13	19	17	4	3	13
$CoPd/Al_2O_3$	67	57	8	4	13	18	9	4	3	16
$CoIr/Al_2O_3$	67	55	10	5	9	18	8	6	7	15
$CoRu/Al_2O_3$	69	57	5	4	15	18	4	3	6	17

In summary, taking the ethanol steam reforming at 400 °C, the $CoRu/Al_2O_3$ catalyst has shown the higher H_2 selectivity with low production of CO.

These results demonstrated that the supported-Co promoted catalysts are highly promising materials for hydrogen production by ethanol steam reforming, but the C_2H_4 selectivity and the coke formation must be reduced. Further studies related to the changes of the alumina support aiming to minimize the acid character are in progress.

4. Conclusions

In this study, the Al_2O_3-supported cobalt catalysts promoted with small amounts of noble metals have been investigated for H_2 production by steam reforming of ethanol. It was observed that the methodology used in the preparation leaded to the formation of Co_3O_4 ($CoO_x{\cdot}Co_2O_3$) spinels, which remained unaltered with the noble metal addition. Moreover, the actual catalyst composition was very close to the nominal formulation for Co (18%), all presenting a homogeneous distribution of this metal. Results of XAS analyses have shown that no significant changes occur in the oxidation states of Co due to noble metals addition. However, a large influence of noble metals on the Co catalyst has been evidenced by TPR. The addition of small amounts of the promoter metals caused a significant decrease on the reduction temperature of Co_3O_4 due to a hydrogen spillover effect. As a result, the reducibilities of these promoted catalysts increased, which should be the main contribution to catalytic effect given by the small amounts of the promoter metals to the cobalt phase.

Experimental tests for the ethanol steam reforming allowed evaluating that the Co/Al_2O_3 promoted catalysts produced a hydrogen-rich gas mixture either at 400 and 500 °C. In the experiments performed at 400 °C, the Co/Al_2O_3 catalyst showed lower H_2 formation and higher C_2H_4 production than those of the promoted catalysts. The larger catalytic performance at 400 °C was obtained for the $CoRu/Al_2O_3$ catalyst, which presented the highest H_2 production with the lowest amount of CO.

Acknowledgements

The authors thank FAPESP and CNPq for financial assistances, Brazilian Synchrotron Laboratory (LNLS) for the XAS experiments and DEQ/UFSCar for BET and XRD analyses.

References

[1] A.D. Qi, S.D. Wang, G.Z. Fu, D.Y. Wu, J. Power Sources 162 (2006) 1254.
[2] R. Farrauto, S. Hwang, L. Shore, W. Ruettinger, J. Lampert, T. Giroux, Y. Liu, O. Ilnich, Annu. Rev. Mater. Res. 33 (2003) 1.
[3] J. Papavasiliou, G. Avgouropoulos, T. Ioannides, Appl. Catal. B 69 (2007) 226.
[4] V. Mas, R. Kipreos, N. Amadeo, M. Laborde, Int. J. Hydrogen Energy 31 (2006) 21.
[5] A. Haryanto, S. Fernando, N. Murali, S. Adhikari, Energy Fuels 19 (2005) 2098.
[6] M. Benito, J.L. Sanz, R. Isabel, R. Padilha, R. Arjona, L. Daza, J. Power Sources 151 (2005) 11.
[7] C. Diagne, H. Idriss, A. Kiennemann, Catal. Commun. 3 (2002) 565.
[8] S. Damyanova, J.M.C. Bueno, Appl. Catal. A 253 (2003) 135.
[9] D.K. Liguras, D. Kondarides, X.E. Verykios, Appl. Catal. B 43 (2003) 345.
[10] H.V. Fajardo, L.F.D. Probst, Appl. Catal. A 306 (2006) 134.
[11] A. Kadouri, C. Mazzocchia, Catal. Commun. 5 (2004) 339.
[12] D.R. Sahoo, S. Vajpai, S. Patel, K.K. Pant, Chem. Eng. J. 125 (2007) 139.
[13] S. Freni, S. Cavallaro, N. Mondello, L. Spadaro, F. Frusteri, Catal. Commun. 4 (2003) 259.
[14] R.K. Santos, M.S. Batista, J.M. Assaf, E.M. Assaf, Quim. Nova. 28 (2005) 587.
[15] F. Haga, T. Nakajima, H. Miya, S. Mishima, Catal. Lett. 48 (1997) 223.
[16] M.S. Batista, R.K.S. Santos, E.M. Assaf, J.M. Assaf, E.A. Ticianelli, J. Power Sources 124 (2003) 99.
[17] M.S. Batista, R.K.S. Santos, E.M. Assaf, J.M. Assaf, E.A. Ticianelli, J. Power Sources 134 (2004) 27.
[18] M.S. Batista, E.M. Assaf, J.M. Assaf, E.A. Ticianelli, Int. J. Hydrogen Energy 31 (2006) 1204.
[19] M. Meng, Y.-Q. Zha, J.-Y. Luo, T.-D. Hu, Y.-N. Xie, T. Liu, J. Zhang, Appl. Catal. A 301 (2006) 145.
[20] M. Meng, P.-Y. Lin, Y.-L. Fu, Catal. Lett. 48 (1997) 213.
[21] D. Xu, W. Li, H. Duan, Q. Ge, H. Xu, Catal. Lett. 102 (2005) 229.
[22] T.K. Das, G. Jacobs, P.M. Patterson, W.A. Conner, J.L. Li, B.H. Davis, Fuel 82 (2003) 805.
[23] G. Jacobs, T.K. Das, P.M. Patterson, J.L. Li, L. Sanchez, B.H. Davis, Appl. Catal. A 247 (2003) 335.
[24] D. Schanke, S. Vada, E.A. Blekkan, A.M. Hilmen, A. Hoff, A. Holmen, J. Catal. 156 (1995) 85.
[25] Ø. Borg, S. Eri, E.A. Blekkan, S. Storsæter, H. Wigum, E. Rytter, A. Holmen, J. Catal. 248 (2007) 89.
[26] C.-B. Wang, C.-W. Tang, H.-C. Tsai, S.H. Chein, Catal. Lett. 107 (2006) 223.
[27] H. Yue, Y.-W. Chen, Mater. Chem. Phys. 85 (2004) 171.
[28] B. Jongsomjit, J. Panpranot, J.G. Goodwin, J. Catal. 204 (2001) 98.
[29] E. Iglesia, S.L. Soled, R.A. Fiato, G.H. Via, J. Catal. 143 (1993) 345.
[30] G. Jacobs, P.M. Patterson, Y. Zhang, T.K. Das, J. Li, B.H. Davis, Appl. Catal. A 233 (2002) 215.
[31] T. Vrålstad, W.R. Glomm, M. Rønning, H. Dathe, A. Jentys, J.A. Lercher, G. Øye, M. Stöcher, J. Sjöblom, J. Phys. Chem. B 110 (2006) 5386.
[32] G. Jacobs, J.A. Chaney, P.M. Patterson, T.K. Das, B.H. Davis, Appl. Catal. A 264 (2004) 203.